Available online at www.sciencedirect.com
ScienceDirect
Geochimica et Cosmochimica Acta 74 (2010) 5398–5409
Geochimica et Cosmochimica Acta
www.elsevier.com/locate/gca

An attempt to characterize phase Q: Noble gas, Raman spectroscopy and transmission electron microscopy in residues prepared from the Allende meteorite

Jun-ichi Matsuda [a,*], Kazuhiko Morishita [a], Hidetomo Tsukamoto [a], Chie Miyakawa [a], Masayuki Nara [b], Sachiko Amari [c], Tetsuya Uchiyama [d], Seiji Takeda [d]

[a] Department of Earth and Space Science, Graduate School of Science, Osaka University, Toyonaka, Osaka 560-0043, Japan
[b] Laboratory of Chemistry, College of Liberal Arts and Sciences, Tokyo Medical and Dental University, Chiba 272-0827, Japan
[c] Laboratory for Space Sciences and the Physics Department, Washington University, St. Louis, MO 63130-4899, USA
[d] Department of Physics, Graduate School of Science, Osaka University, Toyonaka, Osaka 560-0043, Japan

Received 19 March 2010; accepted in revised form 9 June 2010; available online 17 June 2010

Abstract

We have prepared a HF–HCl residue and its oxidized residue of the Allende meteorite and have measured the elemental concentrations and the isotopic compositions of noble gases. In the HF–HCl reside, noble gases are enriched in colloidal fraction compared to the non-colloidal fraction by a factor of 2–4. The heavy noble gases were evidently lost after the oxidization, indicating that phase Q (carrier of planetary heavy noble gases) was removed by the oxidation. The Raman spectroscopic parameters show that the colloidal fraction of the HF–HCl residue is more amorphous compared to the non-colloidal fraction. As the ion irradiation converts carbon into a more amorphous form, our result indicates that the "plasma model" is more plausible than the "labyrinth model" as the origin of phase Q. TEM (Transmission Electron Microscope) observations also show such a trace of ion irradiation. While the TEM observations did not show any large difference between the HF–HCl residue and its oxidized residue, the Raman spectroscopic parameters changed discretely resulting from the oxidization. This observation indicates that the oxidization not only dissolved and removed oxidized carbon, but also changed the carbon structure itself to a more amorphous (disordered) state. The Raman spectroscopic results indicate the possibility that release of Q-gas during oxidation is not accompanied by mass loss and that the release of Q-gas simply resulted from rearrangement of carbon structure during oxidation.

1. INTRODUCTION

Noble gases have played important roles in geochemistry and cosmochemistry (e.g. Ozima and Podosek, 2002). These gases are chemically inert, highly volatile and their behavior is not affected by chemical conditions. Thus, changes in elemental abundances and isotopic compositions of noble gases are mainly controlled by physical conditions, implying that noble gases could be useful tracers in the study of the origin and evolution of the solar system. Hence, noble gas geochemistry has become an important field of earth and planetary sciences.

One of the important and essential topics in noble gas geochemistry is phase Q. Noble gases in a primitive meteorite are not uniformly distributed, but rather are located in a very small portion of the meteorite. Lewis et al. (1975) dissolved the Allende meteorite in HF–HCl and found that the primordial trapped noble gases were retained in the HF–HCl residue (about 0.5% of the bulk meteorite). When they

* Corresponding author. Tel.: +81 6 6850 5495; fax: +81 6 6850 5541.
E-mail address: matsuda@ess.sci.osaka-u.ac.jp (J. Matsuda).

0016-7037/$ - see front matter © 2010 Elsevier Ltd. All rights reserved.
doi:10.1016/j.gca.2010.06.009

further treated the HF–HCl residue with an oxidant like HNO_3, the weight loss by oxidation was only 4–8%, but most of the heavy noble gases (and also some He and Ne) were lost. This minor change in weight indicates that only a small portion of the oxidized material (0.02–0.04% of the bulk meteorite) is the main carrier of the primordial trapped heavy noble gases. They termed this oxidized phase as "Q" for "quintessence". The noble gas in phase Q is isotopically normal and elementally fractionated, being enriched in heavy noble gases compared to the solar component, and was called Q-gas or Type P1 (Huss and Lewis, 1994). Subsequent studies determined that phase Q is a kind of carbonaceous material (Reynolds et al., 1978; Ott et al., 1981), but its chemical state has not been identified. Phase Q is present not only in carbonaceous chondrites, but also in ordinary chondrite (e.g. Moniot, 1980) and the amount of Q-gas decreases with increasing petrologic type, while the median release temperatures increase from 1100 to 1400 °C from CI to H3.6 (Huss et al., 1996). Thus, phase Q is partly destroyed by thermal metamorphism but is still present even in Type 4 ordinary chondrites (Matsuda et al., 2010). Matsuda et al. (2005) reported the presence of phase Q in a graphite nodule even in the Canyon Diablo iron meteorite, indicating that the Q-gases were widely distributed in the early solar system. In principle, the elemental abundances and the isotopic compositions of Q-gases may be determined by comparing the difference between the data before and after oxidation. However, phase Q contributes only minor portions of the He and Ne in the residue and consequently, it is difficult to determine their components accurately. Wieler et al. (1991, 1992) successfully analyzed Q-gases directly using the closed-system etching method. Thus, the elemental abundances and the isotopic compositions of Q-gases may be precisely determined even though the chemical state of phase Q is not well defined. The release temperature of major carbon is different from that of noble gases, indicating that phase Q is a very minor carbon phase. This interpretation is in agreement with the observed mass losses on oxidation (Schelhaas et al., 1990; Verchovsky et al., 2002).

Two types of Q have previously been proposed in the literature. From an oxidation experiment of Allende residues, Gros and Anders (1977) concluded that two Q-phases exist with different noble gas concentrations and oxidation properties. "Q1" contained most of the heavy noble gases and was readily soluble in cold diluted HNO_3, while "Q2" contained heavy noble gases in concentrations at least one order of magnitude lower than in Q1 and was slowly dissolved in hot concentrated HNO_3. Busemann et al. (2000) also reported that phase Q consists of at least two carbonaceous carrier phases "Q_1" and "Q_2". Q_1 has higher He/Xe and Ne/Xe, and releases noble gases by moderate etching, and carries the major portion of Q-gases. In contrast, Q_2 is more resistant to etching. Marrocchi et al. (2005) reported that when the HF–HCl residue from the Orgueil meteorite was treated with pyridine, the low temperature fractions of Q-gases in the residue were lost. They concluded that there was more than one type of Q and that organic Q was destroyed by pyridine treatment. The loss of noble gas with pyridine treatment for Orgueil has been confirmed by Matsuda and Amari (2009). However, Busemann et al. (2008) did not observe a significant difference in noble gas concentrations between pyridine-treated and untreated residues in other primitive meteorites, including Bells (CM2), EET 92042 (CR2), GRO 95577 (CR1) and Murchison (CM2) and concluded that phase Q was not attacked by pyridine. Matsuda et al. (in press) also observed that pyridine treatment did not affect the noble gas concentration in the Allende meteorite. Thus, Orgueil is a special case and it is possible that pyridine simply reacted with a specific organic material that was formed and adsorbed the fractionated Q- and HL-gases during the aqueous alteration in the parent body of Orgueil (Matsuda et al., in press).

Matsuda et al. (1999) reported a fine black material floating on the surface of water during freeze–thaw disaggregation, similar to the HF–HCl residue. The elemental concentrations and most isotopic ratios of noble gases in this fraction indicate that this floating fraction is very similar to the chemical residue except for the $^{129}Xe/^{132}Xe$, which is very high in the latter because of the readsorption of ^{129}Xe from the dissolved minerals during the chemical treatment. This was the first time that a Q-rich fraction was separated utilizing a purely physical method, although the recovered mass fraction is >10 times less than that of the chemical residue (Matsuda et al., 1999). Amari et al. (2003) applied colloidal and density separation techniques to this "floating fraction" C1-8. Among the nine density fractions of C1-8, C1-8D (1.65 ± 0.04 g/cm^3) retained the highest noble gas concentrations; half of the Xe-Q in the sample C1-8 was contained in fraction C1-8D (about 20% by mass of C1-8). Observations by scanning electron microscopy showed that grain sizes of fraction C1-8D ranged from a little less than 1–4 μm and that many grains were present as aggregates of smaller grains forming flower-like shapes. Energy dispersive X-ray spectra showed that most of these grains were carbonaceous (Amari et al., 2003). Matsuda et al. (2009) examined the floating fraction using Raman spectroscopy. We will discuss their results in detail together with our new data in later sections of this contribution.

In this contribution, we use Raman to further investigate the chemical residues of the Allende meteorite. We have prepared the HF–HCl residue (Q-rich) and its oxidized residue (Q-deficient). After confirming the presence of Q-gases in these residues, we examined them using Raman spectroscopy and transmission electron microscope (TEM) to investigate the chemical features of phase Q.

2. SAMPLE PREPARATION

An Allende fragment weighing 4.9154 g was alternately treated with 10 M HF–1 M HCl and 6 M HCl at room temperature to dissolve silicate. The sample was decomposed gradually, following the method developed at the University of Chicago (e.g. Amari et al., 1994). This cycle was repeated several times, and was followed by alternate treatment using 0.6 M H_3BO_3–6 M HCl and 6 M HCl–2 M HF. During the removal of elemental sulfur with CS_2, we found that some material was suspended in the supernatant, although a major part of the fraction was

centrifuged down at the bottom of the tube. The centrifuged fraction (identified as AMD1), was further treated with 0.5 N $Na_2Cr_2O_7$–2 N H_2SO_4 at 75 °C for 10 h to destroy Q, yielding the oxidized residue AMD2. We termed the suspended fraction obtained during the CS_2 treatment as AMD3. The yield of AMD3 was approximately 1/6 of that of AMD1.

3. EXPERIMENTAL RESULTS AND DISCUSSION

3.1. Noble gases

The details of noble gas measurement and the data obtained for this contribution are given in Appendix A. Fig. 1 compares the total elemental concentrations in the original residue (AMD1 and AMD3) and the oxidized residue (AMD2). Argon, Kr and Xe concentrations in the original residue AMD1 are about an order of magnitude higher than those in the oxidized residue AMD2, verifying that the oxidation process removed phase Q. The isotopic data also indicate that that Q-gases were more effectively removed in AMD2 compared to the previous experiment by Lewis et al. (1975; see Appendix A). Noble gas concentrations in AMD3 are ~2–4 times higher than those of AMD1. Previous work with the HF–HCl residues from ordinary H-type chondrites demonstrated that the colloidal fractions of the HF–HCl residue are enriched in the heavy noble gases by a factor 10–30 compared with non-colloidal fractions (Moniot, 1980). In the present study, the colloidal fraction was taken as the suspended material obtained during the CS_2 treatment, whereas the colloid described by Moniot (1980) is the suspended fraction derived from methanol treatment during centrifugation. In both experiments, "colloid" is not a physical-chemistry term in the strictest sense, but simply indicates a suspended material. This suspension is not due to merely the small grain size, but is likely due to the repulsion by the surface charge of the nanodiamonds (Lewis et al., 1989). In fact, we could sediment AMD3 at a lower pH although a true colloid does not settle down by change of pH. The SEM observation confirmed that the main element in AMD1 and AMD3 is carbon. Minor amounts of other elements, Si and Al, were detected for AMD1 but not for AMD3, indicating that AMD3 is pure carbon.

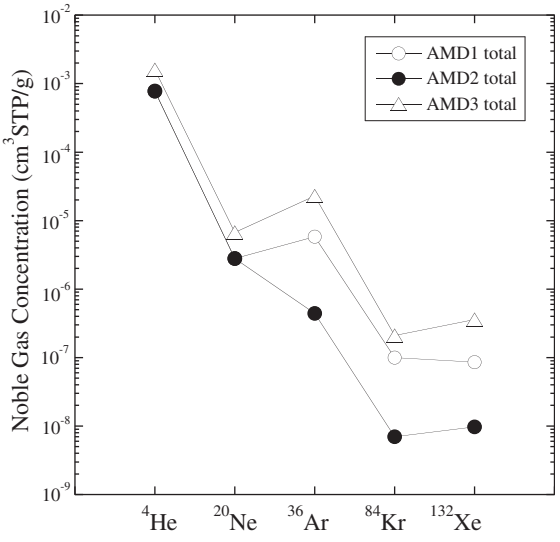

Fig. 1. Noble gas concentrations in the original HF–HCl residue (AMD1 and AMD3) and the oxidized residue (AMD2) prepared from AMD1.

3.2. Raman spectroscopy

3.2.1. Experimental and band fitting

Raman spectroscopic studies were performed using a Raman microscope (Kaiser HoloLab 5000, Kaiser Optical Systems, Inc.) equipped with a 532 nm YAG laser, holographic transmission grating, and a charge-coupled device (CCD) detector. A laser power of 1.2–1.6 mW at the sample surface was utilized throughout this study. The spectral resolution in the present system was approximately 4.8 cm^{-1}. Raman spectra were obtained using 10 accumulations of 30 s each. The laser size was approximately 2 μm in diameter. Raman spectra of disordered graphitic carbon (G band at about 1580 cm^{-1} and D band at about 1350 cm^{-1}) were obtained for all three samples as previously reported for the carbon material in carbonaceous chondrites (Bonal et al., 2006; Busemann et al., 2007). The spectra were corrected for the fluorescence background by subtracting a linear baseline at 1000–2000 cm^{-1} range, which is where Raman peaks of carbon were observed. The spectra were then fitted with two Lorentzian profile curves (Fig. 2). The peak positions (ω_G and ω_D), intensities (I_G and I_D) and the FWHM (full-width at half-maximum; $FWHM_G$ and $FWHM_D$) of the G and D bands were obtained from these curve fittings to define the spectral parameters used to characterize various forms of carbon. The peak position and the FWHM were used as estimates of the degree of disorder.

3.2.2. On the Raman parameters and our previous studies

The G band is assigned to the fundamental E_{2g} vibration mode of the aromatic plane of graphite and only this band is observed in perfectly crystallized graphite. The origin of

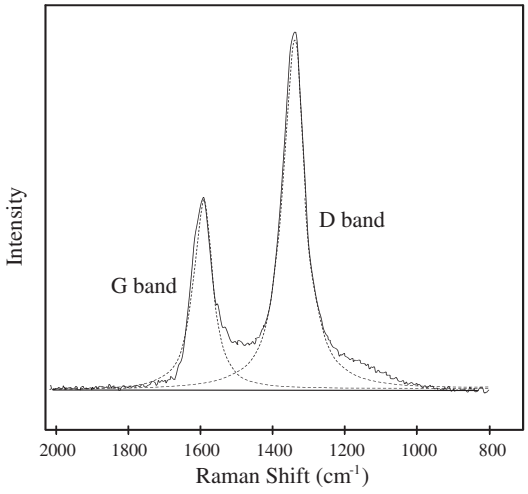

Fig. 2. Typical Raman spectrum in this study and two bands fitting.

the D band in graphite is related to structural defects (D for defect). The D band is observed in graphitic carbon, including activated charcoal, carbon black and vitreous carbon (Tuinstra and Koenig, 1970). The diamond band is at 1332 cm^{-1} and is located close to the D band of graphite (Solin and Ramdas, 1970). A sharp Raman peak seen only at 1332 cm^{-1} is the diamond band. When the D band of graphite and D band of diamond are very broad is often difficult to distinguish the two peaks. However, when a G band is present and the diamond is in nanoscale size, a broad Raman peak ranging upward of 1332 cm^{-1} is regarded as a D band of graphite. This is because the downward shift of the D band position is reported in nanocrystalline diamond (Prawer et al., 2000; Sun et al., 2008). The presolar diamond (the host phase of HL component) in Allende is estimated to be about 3 nm in size (Daulton et al., 1996) and the D band position higher than 1332 cm^{-1} is not diamond.

Using Raman spectroscopy, Matsuda et al. (2009) examined the C1-8D fraction and three additional density fractions, C1-8G (1.97 ± 0.06 g/cm^3), C1-8K (2.2–2.3 g/cm^3) and C1-8J (1.1–1.6 g/cm^3). Each of the latter three samples contained only 5–6% of the Xe-Q found in the C1-8 sample (^{132}Xe concentrations in these samples are about 1/6 to 1/3 of C1-8D). The highest Q-rich fraction C1-8D has the lowest intensity ratios for the D band and G band (I_D/I_G) compared to the other density fractions at the measurement using a low laser power of 0.5 mW. Busemann et al. (2007) reported that Allende plots within the range for nanocrystalline graphite. However, it is unclear whether Allende is in the stage of graphite to nanocrystalline graphite (Stage 1 in Ferrari and Robertson, 2000) or nanocrystalline graphite to amorphous carbon (Stage 2 in Ferrari and Robertson, 2000). The graphitic structure is well developed in Allende carbon. Matsuda et al. (2009) assumed that Allende carbon was in the stage of nanocrystalline graphite to graphite (Stage 1) and concluded that the Q-rich fraction was enriched in graphitic material with larger domain dimensions. However, if the Allende carbon is in the region of Stage 2, the low I_D/I_G simply indicates that the Q-rich fraction is more amorphous. The carbonaceous materials of C1-8 were very sensitive to the laser power utilized during the Raman analyses. For example, the Raman parameters changed at the higher laser power of 2–6 mW, which can be attributed to the effect of laser-induced heating.

Recently, we showed that the power of the laser had a great effect on the Raman parameters of the carbon material, especially for Allende. However, there is no significant difference for Allende residue between the experiments at 0.5 mW and 1.2–1.6 mW; ω_D and ω_G decreased by only about 1 cm^{-1} as the laser power was increased. Thus, we may directly compare our Raman data from the chemical residues measured at a laser power of 1.2–1.6 mW with those obtained previously for the floating fraction at a laser power of 0.5 mW.

3.2.3. The present results of chemical residues and the comparison with those of floating fraction

A plot comparing the positions of the D and G bands, ω_D vs. ω_G, for AMD1, AMD2 and AMD3 shows that ω_D and ω_G for AMD1 are nearly constant at ~1345 cm^{-1} and 1595 cm^{-1}, respectively (Fig. 3a). The ω_G for AMD3 varies from 1585 cm^{-1} to 1596 cm^{-1} although ω_D remains nearly constant at about 1343 cm^{-1}. The peaks for AMD1 and AMD3 (and C1-8) seem to follow the same continuous trend, indicating that our colloidal separation was effective in dividing these two groups. The data points for AMD2 are markedly different from those of AMD1 (and AMD3), and are situated in a discrete and separate location on the plot. C1-8 samples have ω_D values similar to those of AMD1 and AMD3, but have ω_G values higher than those of AMD1 and AMD3. Fig. 3b shows plots of $FWHM_G$ vs. ω_G and in this case, a continuous trend of AMD1, AMD3, AMD2 and C1-8 can be observed. The single inverse correlation of $FWHM_G$ vs. ω_G (Fig. 3b) has been observed in all carbon materials of meteorites (Bonal et al., 2006; Busemann et al., 2007). Thus the trend in Fig. 3b is observed regardless of the sample. However, with plots of $FWHM_D$ vs. ω_D (Fig. 3c) and I_D/I_G vs. ω_G (Fig. 3d), again there are discrete differences in the data positions of AMD2 compared to AMD1.

3.2.4. Comparison of AMD1 and AMD2

Fig. 3a shows that the oxidation process (used on AMD2) shifts both peak positions (ω_G and ω_D) to higher values. Although oxidation does not significantly affect $FWHM_G$ (Fig. 3b), it does broaden the $FWHM_D$ by approximately 50% (Fig. 3c).

Generally, an evolution to amorphous carbon increases $FWHM_G$ and $FWHM_D$ and downshifts the G band peak position (Brunetto et al., 2009). Brunetto et al. (2009) showed that noble gas ion irradiation on the various kinds of soot samples make the samples evolve towards an amorphous carbon phase and confirmed the above features. The irradiation resulting from the high laser power during the Raman analyses of C1-8 series in our previous study (Matsuda et al., 2009) likely produced the amorphization of the samples; increase in $FWHM_G$ and $FWHM_D$ and decrease of ω_G. Although ω_G decreases ω_D increases in Matsuda et al. (2009). The increase of ω_D is the same trend as shown in real meteorite samples toward the disordering carbon (Busemann et al., 2007). With regards to I_D/I_G, the change is not simple. The I_D/I_G initially increases and then decreases as the amorphization (disordering) evolves (Busemann et al., 2007). The former stage is in Stage 1 (graphite to nanocrystalline graphite stage) and the latter is in Stage 2 (nanocrystalline graphite to amorphous carbon stage; Ferrari and Robertson, 2000). The Allende carbon is just in the nanocrystalline region and I_D/I_G decreased after high power laser irradiation for C1-8 samples (Matsuda et al., 2009). This indicates that Allende floating fractions changed to amorphous carbon with the high laser heating.

The oxidation from AMD1 to AMD3 shows complex change where $FWHM_D$ and ω_D increase (Fig. 3c), but $FWHM_G$ decreases and G band peak position slightly increases (Fig. 3b). The former features show the amorphization (graphitic carbon is partly oxidized and/or defect increases), but the latter show the graphitization (highly disordered carbon is oxidized and is dissolved out). It is conceivable that both process of graphitization and

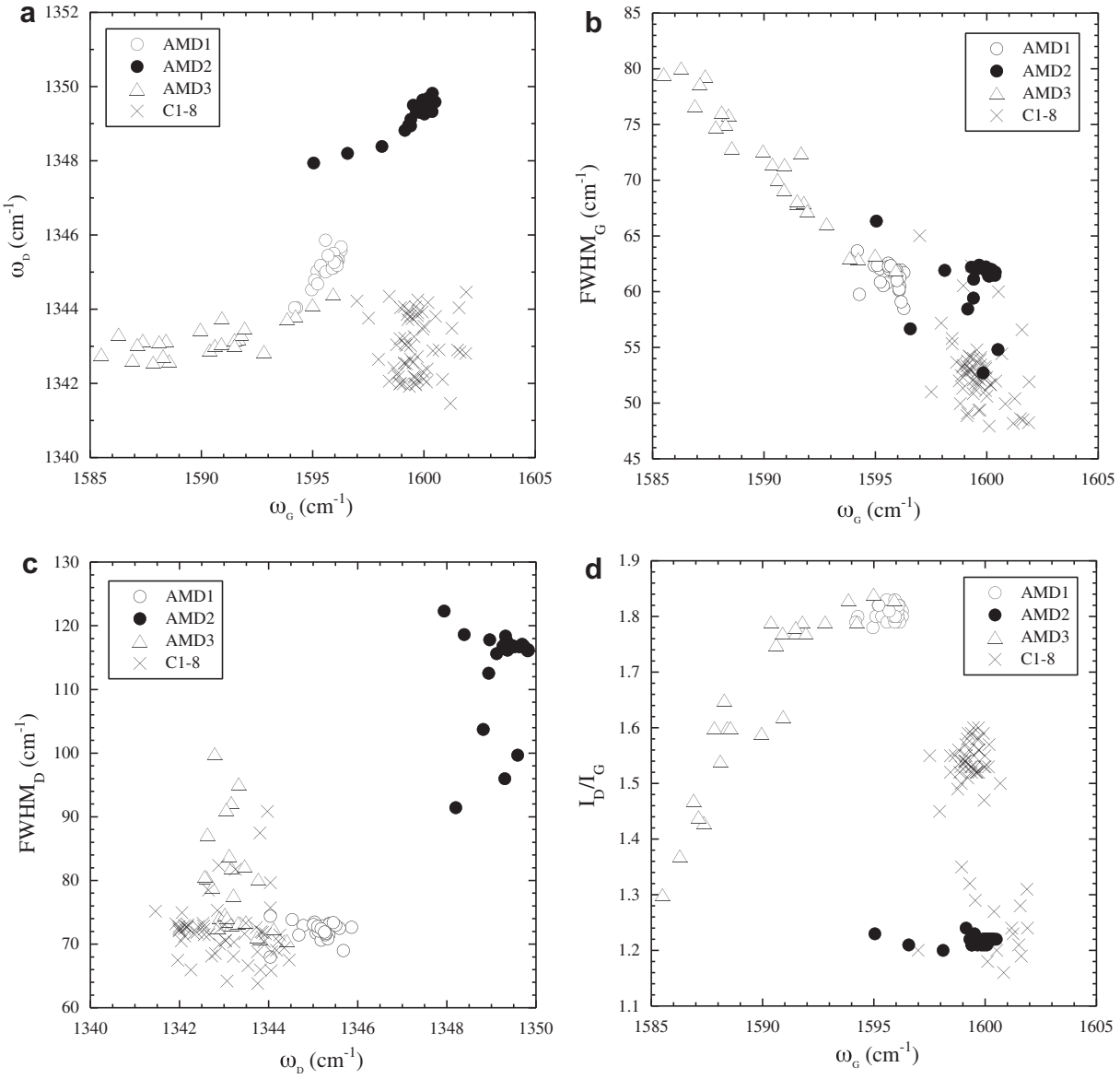

Fig. 3. Comparisons of Raman spectroscopic parameters for samples prepared from the Allende meteorite. (a) ω_D (peak position of D band) against ω_G (peak position of G band) and (b) $FWHM_G$ (full-width at half-maximum of G band) against ω_G, (c) $FWHM_D$ (full-width at half-maximum of D band) against ω_D and (d) I_D/I_G (peak intensity ratio of D and G bands) against ω_G for the original residue (AMD1 and AMD3) and the oxidized residue (AMD2). The sample C1-8 is the floating fraction similar to the original residue, but obtained by a purely physical method (Amari et al., 2003; Matsuda et al., 2009).

amorphization occur at the oxidation. Furthermore, the data points of $FWHM_D$ and ω_D are separated after the oxidation.

The change in peak positions (ω_G and ω_D) during oxidation may be attributed to the fact that the G and D band peaks are combinations of several types of disordered graphitic carbon peaks. It is generally supposed that oxidation simply dissolves out the oxidizable carbon like the refining process removing the remaining graphite from shock-produced diamonds (e.g. Matsuda et al., 1995). The peak position changes if some kinds of carbon contained in the composite peak are removed. In this case, the shift of peak position should be continuous and FWHM should be small, because only some composite peaks have been removed from the original one. However, the shift of ω_D is discrete and $FWHM_D$ is increased from AMD1 to AMD2 after the oxidation (Fig. 3c). These shifts towards higher ω_D are correlated with the increase of $FWHM_D$. These results indicate that the oxidation procedure does not simply dissolve certain types of carbon, resulting in a shift of the peak position, but rather the oxidation process changed the graphitic carbon into a more disordered structure. The upward shift of ω_G and the decrease of $FWHM_G$ (Fig. 3b) indicate that some of the disordered oxidizable carbon was dissolved by oxidation. As the carbon in Allende is not a single component, a complex chemical reac-

tion may have occurred during oxidation. The downward shift of I_D/I_G is compatible with the amorphization from nanocrystalline graphite into amorphous carbon, but can also be explained by the graphitization from nanocrystalline graphite to graphite (Ferrari and Robertson, 2000). The upward shifts in the G band peak position indicate that carbon with long bond lengths of carbon structure and/or disordered (amorphous) carbon are selectively dissolved.

A commonly held belief is that the oxidation procedure used on the HF–HCl residue simply dissolves out the oxidizable carbon material, resulting in a physical loss of the original material, with no change in unoxidized carbon (e.g. Lewis et al., 1975). If this were the case, the data points of AMD2 (oxidized residue of AMD1) should have similar characteristics to those of AMD1 in Fig. 3. However, our data show that the data points of AMD2 are distinct in position and value from those of AMD1 (Fig. 3a, c and d). This observation indicates that the oxidation affected the underlying carbon structure and did not simply dissolve a specific kind of carbon material out of the HF–HCl residue. The change in sample characteristics resulting from aggressive acid digestion have been described in previous contributions (Smith and Buseck, 1981; Garvie and Buseck, 2004).

In Fig. 3d, the data points of the floating fraction C1-8 are distinguished from those in AMD1 and AMD3. The G band position, ω_G, for C1-8 is slightly higher than those for AMD1 and AMD3 by about 5 cm^{-1}, although ω_D is similar (Fig. 3a). This difference is large compared to the effect resulting from differences in laser power (about 1 cm^{-1}). This suggests that HF–HCl treatment also affects the structure of the carbon. However, it is also plausible that the physical separation simply collects specific kinds of carbon and it is not clear whether HF–HCl treatment affects the carbon structure or not. Busemann et al. (2007) compared the CsF residue and HF–HCl residues from a Raman study and concluded that for the Allende meteorite, the chemical procedure chosen to produce the carbonaceous residues did not significantly affect the Raman results.

3.2.5. Comparison of AMD1 and AMD3 and its implication

Both AMD1 and AMD3 are original residues, but AMD3 has noble gas concentrations higher than those of AMD1 by a factor of approximately 2–4. In Fig. 3, the data positions of AMD1 and AMD3 are distinguished. The Raman parameters of AMD3 indicate that it is more amorphous compared to AMD1; low ω_G and large $FWHM_G$ (Fig. 3b) and also large $FMHM_D$ in AMD3 (Fig. 3c). The I_D/I_G of AMD3 are also lower than those of AMD1. These results suggest that Q-gases are enriched in amorphous (disordered) carbon. In Matsuda et al. (2009), the most Q-gas enriched fraction C1-8D also has low I_D/I_G, leading to the opposite conclusion; the phase Q is enriched in graphitic carbon having larger domain size. As there is no difference in ω_G nor $FWHM_G$ among the different density fractions of C1-8, we simply concluded here that Q-gases are enriched in the graphitic carbon having larger domain size compared to the major carbon. This opposing conclusion is based on the assumption that Allende carbon is in the Stage 1 between nanocrystalline graphite to graphite (Ferrari and Robertson, 2000; Casiraghi et al., 2005). However, if Allende carbon is in Stage 2 between nanocrystalline graphite to amorphous carbon, the low I_D/I_G of carbon simply indicates that it is more amorphous (Ferrari and Robertson, 2000; Casiraghi et al., 2005).

For a model of phase Q, Matsuda and Yoshida (2001) previously proposed the "plasma model" where the noble gas ions were implanted into the surface of presolar diamond. The implanted gases can then be removed by nitric acid. The ionized noble gases are highly fractionated, being enriched in heavy noble gases, because of the lower ionization energy of heavier noble gases under plasma conditions. The noble gases are tightly implanted on the carbon and consequently have high release temperatures. This plasma model can better explain the high temperature release of Q-gases than the well-accepted "labyrinth model" (Wacker et al., 1985; Zadnik et al., 1985; Wacker, 1989), whereby the noble gases are trapped in the labyrinth of micropores of carbonaceous matter after being adsorbed on the surface. Ion irradiations of soot (Brunetto et al., 2009) and of diamond (Orwa et al., 2000) show that the carbon samples evolve toward an amorphous carbon phase; broadening of $FWHM_G$ and downshift of ω_G. Thus, the features of our Raman spectra of AMD3 are compatible with these characteristics and support the "plasma model"; phase Q is an amorphous phase of carbon due to noble gas irradiation.

3.3. Transmission electron microscopy (TEM)

Transmission electron microscopy (TEM) was performed at Osaka University using an electron microscope (FEI Tecnai F20) operated at 200 kV.

3.3.1. Previous TEM work

TEM images of original HF–HCl residues of Allende, documented in previous scientific contributions, show curved and tangled graphene sheets, with fringe distances of approximately 0.385 nm (Smith and Buseck, 1981; Harris et al., 2000; Vis et al., 2002; Harris and Vis, 2003). The increase above the 0.337 nm of the pure graphite stacking was attributed to turbostratic stacking. Based on these features, the carbon in the Allende meteorite may be characterized as "poorly graphitized carbon" or "turbostratic carbon" (Vis et al., 2002). These TEM observations are compatible with the "nanocrystalline graphite" estimated from the Raman study of Busemann et al. (2007). Disordered graphitic carbon with porous microstructure has also been observed in the Kainsaz CO3 carbonaceous chondrite (Remusat et al., 2008) and in other CV and CO (Aoki and Akai, 2008). Compared to the carbonaceous materials in CI and CM, graphitization likely occurs in Type 3 carbonaceous chondrite (Aoki and Akai, 2008; Remusat et al., 2008).

Although TEM observations of HF–HCl residues of carbonaceous chondrites have been reported by many researchers, there are only few observations on oxidized residues. In an oxidized residue of Allende, Smith and Buseck (1981) observed graphitic crystallites with a well-ordered concentric structure that amounted to several percent of the sample and stated that such grains were not seen in the original HF–HCl residue.

3.3.2. Present results and implications

We made TEM observation on several grains of AMD1 and AMD3, but the TEM images are more or less similar for each sample. A typical TEM image of AMD1 is shown in Fig. 4a. The TEM images obtained in the present study for AMD1 are similar to the previously published images (Smith and Buseck, 1981; Harris et al., 2000; Vis et al., 2002; Harris and Vis, 2003). Curved graphene sheets with about a 0.34 nm interlayer spacing of graphite and their closed rolled structures were also observed (Fig. 4a).

Our TEM image of the oxidized residue AMD2 (Fig. 4b) shows no large differences in comparison with that of the HF–HCl residue AMD1. Curved graphene sheets are also predominant in AMD2. The only difference between AMD1 and AMD2 is the diffraction pattern of diamond in AMD2, and the ability to observe the 0.21 nm spacing lattice fringes corresponding to the diamond (1 1 1) plane. Similar 0.21 nm spacing is also seen in AMD1 but it is not widely distributed. Nanodiamonds and carbonaceous globules are common in carbonaceous chondrites (Aoki and Akai, 2008). In AMD2, we observed the graphene rolled structure (porous microtexture; Fig. 4c) that was also observed in AMD1, but we could not detect graphitic crystallites as reported by Smith and Buseck (1981). The oxidized residue used in Smith and Buseck (1981) was prepared by HNO_3 but our sample was treated with 0.5 N $Na_2Cr_2O_7$–2 N H_2SO_4. Thus, the different oxidant may have changed the nature of the carbon structure. Another possibility suggested previously by Harris et al. (2000) is that Smith and Buseck's graphite particle in the oxidized residue of Allende is a contaminant from the carbon support films. Thus, we conclude that the HF–HCl residue and its oxidized residue are not so different from each other under our TEM observations, except for the easier detection of diamond in AMD2.

Harris et al. (2000) and Vis et al. (2002) proposed that the closed graphite structure on the nm scale could be a candidate for the carrier of planetary gas (phase Q). Garvie and Buseck (2004) also observed the presence of hollow nanospheres in CM chondrites and suggested that these nanosized carbon grains could be hosts of primordial noble gases (phase Q). Nakamura et al. (2002) suggested that hydrothermal processing of UV-irradiated organics into insoluble droplets resulted in the formation of the hollow nanospheres. However, Remusat et al. (2008) noted that such nanoscale globules most likely are remnant templates of oxide grains lost during sample preparation. Meanwhile, a similar closed carbon structure has also been produced artificially by electron-beam irradiation (Ugarte, 1992). Thus, if the third hypothesis is correct the presence of closed carbon structure also favors the "plasma model" for phase Q, because ionization and implantation are the main mechanism for trapping noble gases in this model. We conclude that ion implantations during plasma process created such nanoscale globules and amorphous carbon (phase Q). Similar closed carbon structures are also observed in AMD2. Thus, we consider that carbonaceous nanoglobules themselves are not the host site of the heavy noble gas (phase Q).

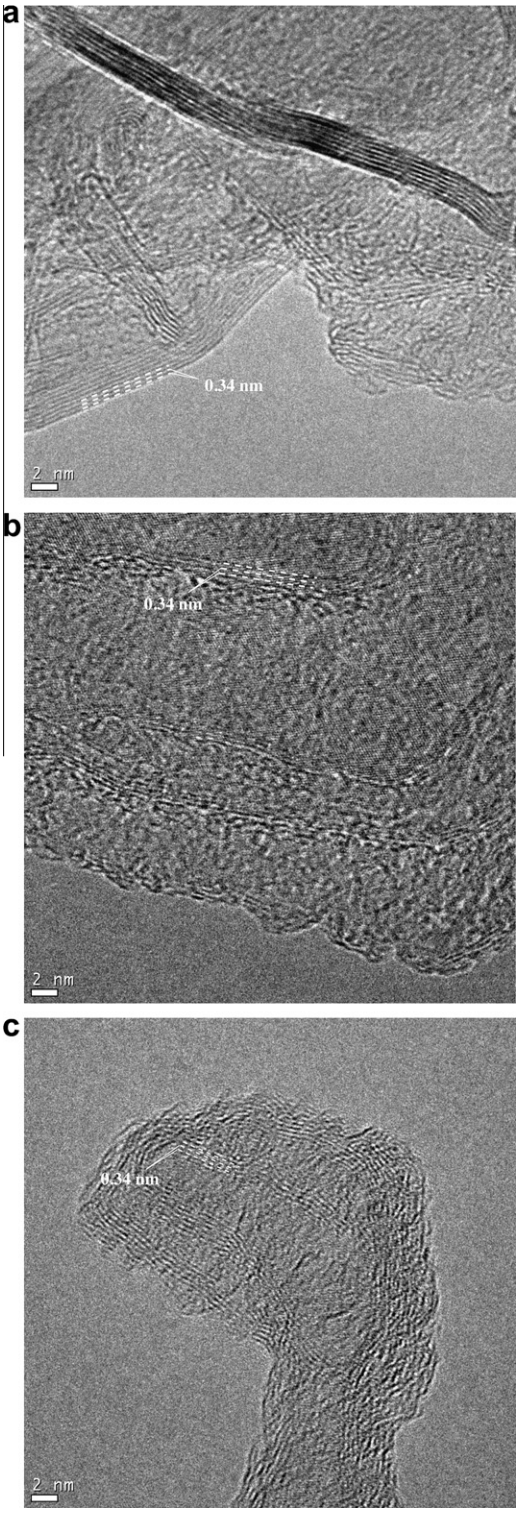

Fig. 4. Typical TEM images of samples prepared from the Allende meteorite. (a) AMD1, (b) AMD2 and (c) onion-like closed carbon structure in AMD2.

4. CONCLUSIONS

From the comparison of colloidal and non-colloidal fractions of the HF–HCl residue of Allende, we found that

the former has noble gas concentrations 2–4 times higher than the latter. Raman spectroscopic characteristics indicate that the colloidal fraction has more amorphous (disordered) carbon compared to the non-colloidal fraction. It is known that the ion implantation evolves the carbon toward amorphous (disordering) carbon. Thus, we consider that the plasma model is plausible for the origin of phase Q. TEM observation also shows the structural features of ion irradiation in the residues.

Another implication from this study is that the chemical treatment like oxidation changes the carbon structure into a more disordered stage. Phase Q is defined as the phase that contains most of heavy noble gases in a meteorite, and is lost during oxidation. Our Raman observation shows that the oxidation process changes the carbon structure into more disordered state. Thus, the release of Q-gas likely resulted from the structural change within the carbon material in the HF–HCl residue. It is likely that the amorphization resulting from chemical treatment is different from that produced by ion irradiation. Additionally, disordering by oxidation releases the gases implanted at the disordered sites.

Ott et al. (1981) and Ott (2002) also proposed that the gas release is caused by a structural rearrangement, although he did not produce any experimental evidence. Thus, our Raman study presented here may provide experimental support for this model. The weight loss of the HF–HCl residue after oxidation is generally very small (e.g. 4–8%). It is likely that this resulted simply from mass loss during the sample treatment (for example, during transfer and

Table A1
Concentrations and isotopic ratios of He, Ne and Ar in the Allende HF–HCl residues (AMD1 and AMD3) and the oxidized residue of AMD1 (AMD2).

Sample	Temp. (°C)	[^{4}He] (10^{-6} cm^3 STP/g)	^{3}He/^{4}He (10^{-4})	[^{22}Ne] (10^{-8} cm^3 STP/g)	^{20}Ne/^{22}Ne	^{21}Ne/^{22}Ne	[^{36}Ar] (10^{-8} cm^3 STP/g)	^{38}Ar/^{36}Ar	^{40}Ar/^{36}Ar
AMD1	600	20	7.13 ± 0.23	0.37	7.46 ± 0.18	0.2494 ± 0.0083	39	0.1894 ± 0.0016	199.6 ± 4.2
(1.55 mg)	1600	760	1.70 ± 0.05	34	8.33 ± 0.09	0.0663 ± 0.0006	540	0.1878 ± 0.0004	0.48 ± 0.04
	Total	780	1.84 ± 0.05	34	8.32 ± 0.09	0.0683 ± 0.0006	580	0.1879 ± 0.0004	14.1 ± 0.3
AMD2	600	110	3.13 ± 0.26	0.75	7.78 ± 0.15	0.1355 ± 0.0032	4.0	0.1884 ± 0.0009	79.4 ± 3.3
(2.34 mg)	1600	660	1.72 ± 0.14	34	8.13 ± 0.17	0.0804 ± 0.0012	40	0.2066 ± 0.0006	9.58 ± 0.43
	Total	770	1.93 ± 0.13	35	8.12 ± 0.16	0.0816 ± 0.0012	44	0.2049 ± 0.0006	15.95 ± 0.49
AMD3	600	32	4.25 ± 0.18	2.0	9.11 ± 0.44	0.0878 ± 0.0099	290	0.1918 ± 0.0005	22.76 ± 0.63
(0.05 mg)	1600	1500	1.45 ± 0.05	77	8.50 ± 0.10	0.0336 ± 0.0012	2000	0.1896 ± 0.0004	0.94 ± 0.09
	Total	1600	1.51 ± 0.05	79	8.52 ± 0.10	0.0350 ± 0.0012	2300	0.1899 ± 0.0004	3.67 ± 0.11
Q[a]			1.23–1.59		10.05–10.70	0.0291–0.0321		0.18727	
HL[b]			1.70		8.5	0.036		0.2270	
Air			0.01399		9.80	0.029		0.188	295.5

[a] Busemann et al. (2000).
[b] Huss and Lewis (1994). This HL component of Ne (Ne-HL) is actually Ne-A2 (Ne-HL + P3) (Huss et al., 1996).

Table A2
Concentrations and isotopic ratios of Kr in the Allende HF–HCl residues (AMD1 and AMD3) and the oxidized residue of AMD1 (AMD2).

Sample	Temp. (°C)	[^{84}Kr] (10^{-10} cm^3 STP/g)	^{78}Kr/^{84}Kr	^{80}Kr/^{84}Kr	^{82}Kr/^{84}Kr	^{83}Kr/^{84}Kr	^{86}Kr/^{84}Kr
AMD1 (1.55 mg)	600	470	0.0057 ± 0.0004	0.0383 ± 0.0012	0.2030 ± 0.0029	0.2006 ± 0.0042	0.3033 ± 0.0036
	1600	570	0.0061 ± 0.0001	0.0402 ± 0.0003	0.2084 ± 0.0008	0.2085 ± 0.0010	0.3203 ± 0.0009
	Total	1000	0.0059 ± 0.0002	0.0393 ± 0.0006	0.2060 ± 0.0014	0.2049 ± 0.0020	0.3126 ± 0.0017
AMD2 (2.34 mg)	600	14	0.0070 ± 0.0011	0.0511 ± 0.0043	0.2063 ± 0.0103	0.1954 ± 0.0091	0.3132 ± 0.0134
	1600	56	0.0036 ± 0.0005	0.0336 ± 0.0015	0.1599 ± 0.0033	0.2029 ± 0.0045	0.3512 ± 0.0052
	Total	70	0.0042 ± 0.0004	0.0371 ± 0.0015	0.1691 ± 0.0033	0.2014 ± 0.0041	0.3436 ± 0.0049
AMD3 (0.05 mg)	600	470	0.0051 ± 0.0008	0.0421 ± 0.0016	0.1956 ± 0.0106	0.2069 ± 0.0072	0.3004 ± 0.0029
	1600	1600	0.0059 ± 0.0005	0.0375 ± 0.0014	0.2039 ± 0.0033	0.1989 ± 0.0032	0.3045 ± 0.0047
	Total	2100	0.0058 ± 0.0004	0.0385 ± 0.0011	0.2020 ± 0.0035	0.2007 ± 0.0030	0.3036 ± 0.0037
Q[a]			0.00603	0.03937	0.2018	0.2018	0.3095
HL[b]			0.0043	0.0308	0.1600	0.1993	0.3603
Air			0.006087	0.03960	0.20217	0.20136	0.30524

[a] Busemann et al. (2000).
[b] Huss and Lewis (1994).

evaporation of the sample material). In fact, the amount of weight lost varies in different experiments (Ott, 2002).

It is likely that phase Q is not an unique, independent carrier, but is the amorphous site of the carbon. Thus, the release of Q-gas simply resulted from the structural disordering rearrangement of the carbon phase. This model provides an explanation for why no one has succeeded in separating pure phase Q for almost 35 years despite numerous attempts and great effort. Furthermore, Raman parameters of carbon residues from different chondrites are discretely distributed (Busemann et al., 2007) even though all these unequilibrated chondrites have phase Q. This observation indicates that a universal phase Q may not be detectable by Raman spectroscopy even though phase Q is an independent and universal entity in these chondrites. Of course, we cannot rule out the possibility that phase Q consists of very fine grains of a discrete phase and that it is always covered by the major disordered graphitic carbon during the Raman spectroscopy observation. However, it is likely that the amorphization and structural rearrangement resulting from oxidation is strongly related with the release of Q-gases.

ACKNOWLEDGMENTS

This research was supported by a Grant-in-Aid for Scientific Research 18104010 (J.M.) and NASA Grant NNG06GF46G (S.A.). We thank Drs. H. Busemann, A.B. Verchovsky, U. Ott and S.V.S. Murty for their comments on the manuscript, the manuscript has been greatly improved by their valuable comments. Thanks are also given to C. Koeberl (handling editor) for his suggestions with regards to preparation of the revised manuscript.

APPENDIX A

A.1. Noble gases

Noble gas measurements were carried out at Osaka University with gas extraction at 600 and 1600 °C using a sector-type mass spectrometer VG5400. We have previously published the details of the gas purification and the measurements (Matsuda et al., 2005; Nishimura et al., 2008). All the sample data were blank-corrected based on hot blanks measured prior to the sample analysis. Measured typical hot blanks at 1600 °C were as follows: $^{4}He = 3.9 \times 10^{-10}$, $^{22}Ne = 2.5 \times 10^{-13}$, $^{36}Ar = 3.8 \times 10^{-12}$, $^{84}Kr = 2.0 \times 10^{-13}$, $^{132}Xe = 3.0 \times 10^{-14}$ cm^3 STP. Blank corrections were negligible for all data except for Kr in AMD3 where they were as high as approximately 25%.

Tables A1–A3 show the results of noble gas concentrations and isotopic ratios. The errors of the noble gas concentrations are ~10%, including the error of the line volume for AMD1 and AMD2. Because of the small sample weight of AMD3, the errors of the concentrations in this sample are about 50%, mainly due to the large error of ±0.02 mg of the sample weight (0.05 mg).

We compared the concentrations of noble gases in our original HF–HCl residues (AMD1 and AMD3) with those in some other original residues of Allende obtained by other authors (Fig. A1). The concentrations of noble gases are

Table A3
Concentrations and isotopic ratios of Xe in the Allende HF–HCl residues (AMD1 and AMD3) and the oxidized residue of AMD1 (AMD2).

Sample	Temp. (°C)	[^{132}Xe] (10^{-10} cm^3 STP/g)	^{124}Xe/^{132}Xe	^{126}Xe/^{132}Xe	^{128}Xe/^{132}Xe	^{129}Xe/^{132}Xe	^{130}Xe/^{132}Xe	^{131}Xe/^{132}Xe	^{134}Xe/^{132}Xe	^{136}Xe/^{132}Xe
AMD1 (1.55 mg)	600	73	0.0040 ± 0.0004	0.0032 ± 0.0003	0.0772 ± 0.0015	1.794 ± 0.021	0.1492 ± 0.0026	0.8009 ± 0.0078	0.3899 ± 0.0072	0.3110 ± 0.0058
	1600	790	0.0048 ± 0.0001	0.0040 ± 0.0001	0.0839 ± 0.0009	1.102 ± 0.009	0.1635 ± 0.0012	0.8263 ± 0.0033	0.4016 ± 0.0045	0.3465 ± 0.0039
	Total	860	0.0048 ± 0.0001	0.0040 ± 0.0001	0.0833 ± 0.0009	1.161 ± 0.009	0.1623 ± 0.0011	0.8241 ± 0.0031	0.4006 ± 0.0042	0.3435 ± 0.0036
AMD2 (2.34 mg)	600	9.9	0.0045 ± 0.0010	0.0032 ± 0.0011	0.0767 ± 0.0058	2.141 ± 0.063	0.1447 ± 0.0076	0.8235 ± 0.0289	0.4246 ± 0.0194	0.3541 ± 0.0258
	1600	87	0.0067 ± 0.0005	0.0059 ± 0.0006	0.0879 ± 0.0067	1.120 ± 0.012	0.1528 ± 0.0024	0.8348 ± 0.0096	0.5546 ± 0.0211	0.6474 ± 0.0170
	Total	97	0.0065 ± 0.0005	0.0056 ± 0.0005	0.0868 ± 0.0060	1.225 ± 0.013	0.1520 ± 0.0023	0.8336 ± 0.0091	0.5413 ± 0.0190	0.6173 ± 0.0155
AMD3 (0.05 mg)	600	470	0.0047 ± 0.0008	0.0051 ± 0.0008	0.0697 ± 0.0032	1.447 ± 0.028	0.1558 ± 0.0043	0.8251 ± 0.0073	0.3820 ± 0.0092	0.3089 ± 0.0083
	1600	3200	0.0055 ± 0.0002	0.0040 ± 0.0003	0.0808 ± 0.0013	1.099 ± 0.012	0.1594 ± 0.0014	0.8247 ± 0.0050	0.3895 ± 0.0049	0.3370 ± 0.0043
	Total	3600	0.0054 ± 0.0002	0.0041 ± 0.0003	0.0794 ± 0.0012	1.144 ± 0.011	0.1589 ± 0.0013	0.8248 ± 0.0044	0.3885 ± 0.0044	0.3333 ± 0.0039
Q[a]			0.00455	0.004057	0.0822	1.042	0.1619	0.8185	0.3780	0.3164
HL[b]			0.00842	0.00569	0.0905	1.056	0.1544	0.8442	0.6361	0.7000
Air			0.003537	0.003300	0.07136	0.9832	0.1514	0.7890	0.3879	0.3294

[a] Busemann et al. (2000).
[b] Huss and Lewis (1994).

variable; those of the colloidal fraction AMD3 are almost identical with those in BA obtained by Wieler et al. (1991), except for ^{4}He and ^{132}Xe which are similar to those in 3C1 (Lewis et al., 1975), whereas those in AMD1 are identical with those (only ^{20}Ne, ^{84}Kr and ^{132}Xe) in 1CSa obtained by Srinivasan et al. (1978). As the mass yield of 1CSa was twice as high as that of the 3C series, it is suggested that 1CSa still contained material other than carbon like AMD1. Fig. A1 also compares the noble gas concentration in the oxidized residue AMD2 with those in the similar oxidized residue 3C2 prepared by Lewis et al. (1975). The noble gas concentrations in our oxidized residue AMD2 are lower than those in 3C2, indicating that Q-gases have been more effectively removed in our oxidized residue. This result is also supported from the Xe isotopic ratios; the ^{136}Xe/^{132}Xe ratio in AMD2 (0.6173) is much higher than that of 3C2 (0.4611), indicating that the concentration of presolar diamond (host phase of Xe-HL) in AMD2 is about two times higher than that in 3C2. The ^{132}Xe-HL fraction in total ^{132}Xe in AMD2 is estimated to be 78%.

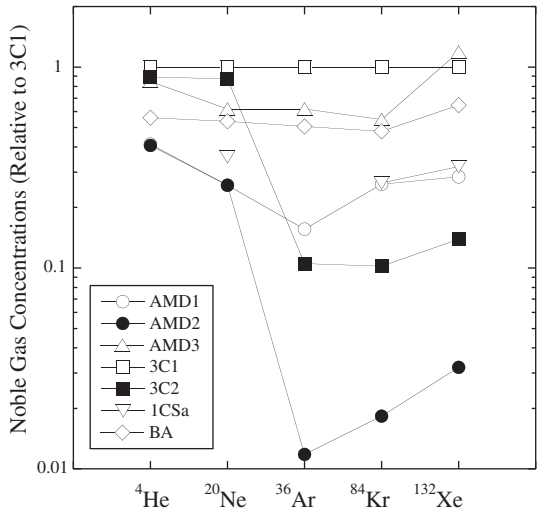

Fig. A1. A comparison of the noble gas concentrations in our original residues (AMD1 and AMD3) and the oxidized residue (AMD2) with those in other original residues; 3C1 (Lewis et al., 1975), BA (Wieler et al., 1991) and 1CSa (only ^{20}Ne, ^{84}Kr and ^{132}Xe; Srinivasan et al., 1978) and the oxidized residue 3C2 (Lewis et al., 1975). The noble gas concentrations are normalized to those in 3C1.

In a Ne three-isotope plot (Fig. A2), AMD1 and AMD2 show the presence of a small amount of cosmogenic component (especially at 600 °C), which is consistent with the observation that AMD1 still contains small amounts of silicate. The low temperature data points also suggest the contribution of air. The data point of the total of AMD3 is identical with that of HL, which is the same as BA and 3C2. The contribution of Ne-Q in the HF–HCl residue is very small because the Q-gas is highly fractionated, being depleting in Ne. Ne-HL is predominant even in the original residue.

Fig. A3 is the three-isotope plot of Ar, where low temperature fractions of our residue show contribution from Ar in air, but the totals (almost the same as the 1600 °C fraction) of AMD1 and AMD3 are similar to Q. The total data point of AMD2 shifts toward the HL component, which resulted from the removal of phase Q from AMD1. The shift of AMD2 toward HL is larger than that of

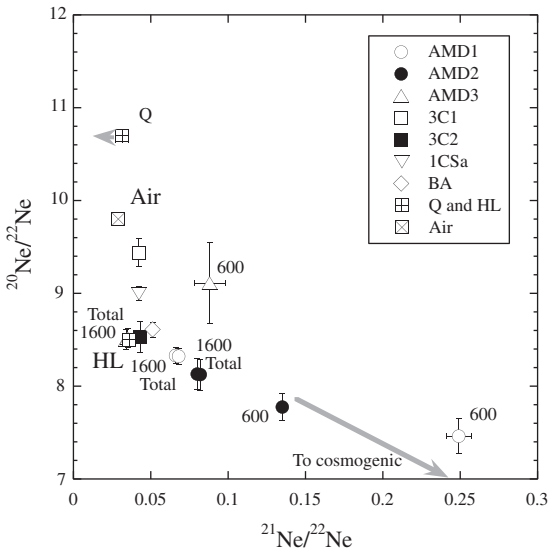

Fig. A2. Neon three-isotope plot for the original residues (AMD1 and AMD3) and the oxidized residue (AMD2) as compared to those in other original and oxidized residues of Allende prepared by other authors; 3C1 (Lewis et al., 1975), BA (Wieler et al., 1991), 1CSa (Srinivasan et al., 1978). The Allende Q composition from Wieler et al. (1991) is shown although Ne-Q has a range (Table A1), and HL is from Huss and Lewis (1994).

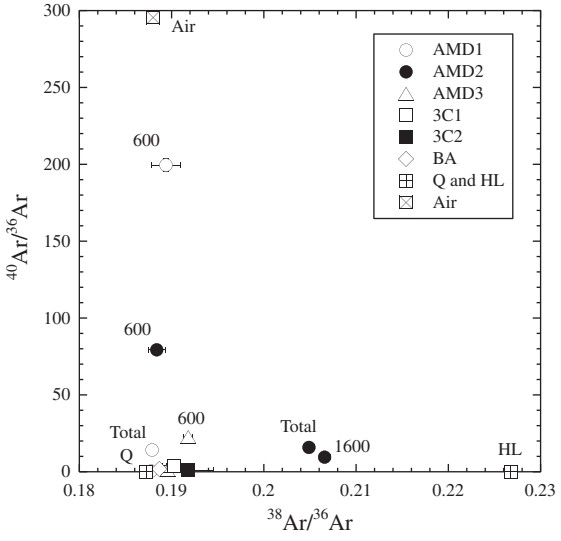

Fig. A3. Argon three-isotope plot for the original residues (AMD1 and AMD3) and the oxidized residue (AMD2) as compared with those from other original and oxidized residues of Allende prepared by other authors; 3C1 (Lewis et al., 1975) and BA (Wieler et al., 1991). For 1CSa (Srinivasan et al., 1978) no Ar data has been reported. The data points of Q and HL are from Busemann et al. (2000) and Huss and Lewis (1994), respectively; their ^{40}Ar/^{36}Ar are very low.

3C2, indicating that the removal of phase Q is more prominent in our experiment, as shown in Xe isotopes.

Fig. A4 illustrates the Kr and Xe isotopic patterns relative to the solar component. Here, Kr and Xe patterns of AMD2 are closer to those of HL as compared with those of 3C2 except for the $^{80}Kr/^{84}Kr$ (Fig. A4a), again indicating that phase Q has been effectively removed from AMD1 by oxidation. The high $^{80}Kr/^{84}Kr$ ratio of total AMD2 reflects the high $^{80}Kr/^{84}Kr$ (0.0511) of the 600 °C fraction (Table A2). The $^{80}Kr/^{84}Kr$ of the 1600 °C fraction is as low as 0.0336. The high $^{80}Kr/^{84}Kr$ of the low temperature fraction may be attributed to the neutron capture on Br: $^{79}Br(n, \gamma\beta)^{80}Kr$. The $^{80}Kr/^{82}Kr$ production rate by neutron capture on Br is about three (Murty and Marti, 1987). Thus, although the neutron capture effect is detectable in the $^{80}Kr/^{84}Kr$ of 600 °C fraction of AMD2, the expected excess of $^{82}Kr/^{84}Kr$ by neutron capture on Br is too small to be obscured. A $^{80}Kr/^{84}Kr$ as high as 0.04052 has also been reported for the lowest temperature fraction in 3CS2 (a coarse fraction of the oxidized residue) by Lewis et al. (1975). Considering that the total ^{84}Kr concentration of 3CS2 is about three times higher than that of AMD2, it is not surprising that the effect of neutron capture is more clearly visible in our sample. It is also difficult to detect neutron capture signature in AMD1 because the ^{84}Kr concentration in the 600 °C fraction of AMD1 is higher than that of AMD2 by a factor of 34.

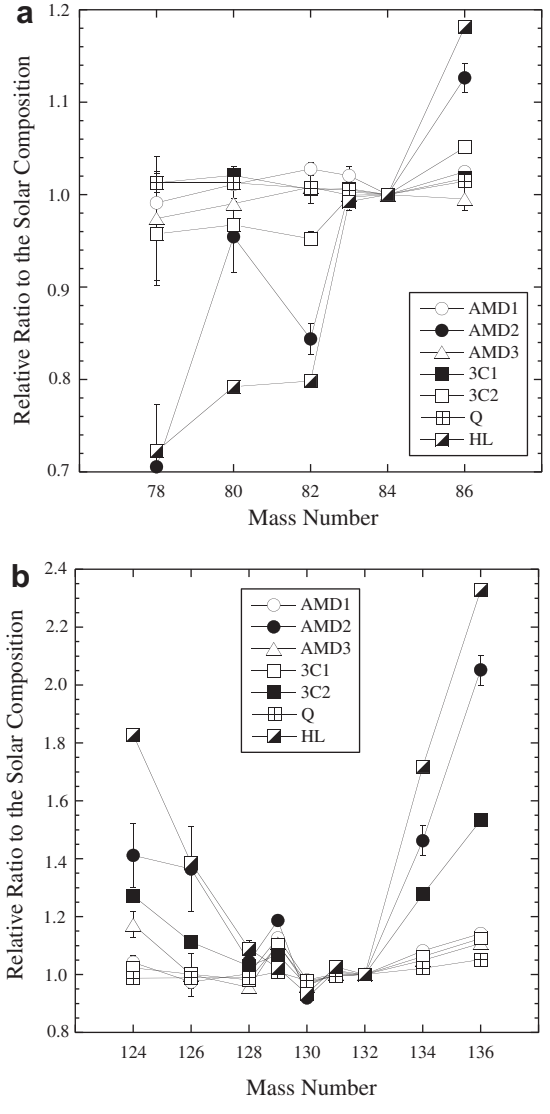

Fig. A4. (a) Kr and (b) Xe isotopic patterns of the original residues (AMD1 and AMD3) and the oxidized residue (AMD2) prepared from the Allende meteorite relative to the solar composition (Anders and Grevesse, 1989), and compared to those in 3C1 and 3C2 (Lewis et al., 1975).

REFERENCES

Amari S., Lewis R. S. and Anders E. (1994) Interstellar grains in meteorites: I. Isolation of SiC, graphite, and diamond; size distributions of SiC and graphite. *Geochim. Cosmochim. Acta* **58**, 459–470.

Amari S., Zaizen S. and Matsuda J. (2003) An attempt to separate Q from the Allende meteorite by physical methods. *Geochim. Cosmochim. Acta* **67**, 4665–4677.

Anders E. and Grevesse N. (1989) Abundances of the elements: meteoritic and solar. *Geochim. Cosmochim. Acta* **53**, 197–214.

Aoki T. and Akai J. (2008) Carbon materials in Antarctic and nonAntarctic carbonaceous chondrites: high-resolution transmission electron microscope. *J. Mineral. Petrol. Sci.* **103**, 173–182.

Bonal L., Quirico E., Bourot-Denise M. and Montagnac G. (2006) Determination of the petrologic type of CV3 chondrites by Raman spectroscopy of included organic matter. *Geochim. Cosmochim. Acta* **70**, 1849–1863.

Brunetto R., Pino T., Dartois E., Cao A.-T., d'Hendecourt L., Strazzulla G. and Bréchignac Ph. (2009) Comparison of the Raman spectra of ion irradiated soot and collected extraterrestrial carbon. *Icarus* **200**, 323–337.

Busemann H., Baur H. and Wieler R. (2000) Primordial noble gases in "phase Q" in carbonaceous and ordinary chondrites studied by closed-system stepped etching. *Meteorit. Planet. Sci.* **35**, 949–973.

Busemann H., Alexander C. M. O'D. and Nittler L. R. (2007) Characterization of insoluble organic matter in primitive meteorites by microRaman spectroscopy. *Meteorit. Planet. Sci.* **42**, 1387–1416.

Busemann H., Alexander C. M. O'D., Nittler L. R. and Wieler R. (2008) Noble gases in insoluble organic matter in the very primitive meteorites Bells, EET92042 and GRO 95577. *39th Lunar Planet. Sci. Conf. CD-ROM*. #1777 (abstr.).

Casiraghi C., Ferrari A. C. and Robertson J. (2005) Raman spectroscopy of hydrogenated amorphous carbons. *Phys. Rev. B* **72**, 085401.

Daulton T. L., Eisenhour D. D., Bernatowicz T. J., Lewis R. S. and Buseck P. R. (1996) Genesis of presolar diamonds: comparative high-resolution transmission electron microscopy study of meteoritic and terrestrial nano-diamonds. *Geochim. Cosmochim. Acta* **60**, 4853–4872.

Ferrari A. C. and Robertson J. (2000) Interpretation of Raman spectra of disordered and amorphous carbon. *Phys. Rev. B* **61**, 14095–14107.

Garvie L. A. J. and Buseck P. R. (2004) Nanosized carbon-rich grains in carbonaceous chondrite meteorites. *Earth Planet. Sci. Lett.* **224**, 431–439.

Gros J. and Anders E. (1977) Gas-rich minerals in the Allende meteorite: attempted chemical characterization. *Earth Planet. Sci. Lett.* **33**, 401–406.

Harris P. J. F. and Vis R. D. (2003) High-resolution transmission electron microscopy of carbon and nanocrystals in the Allende meteorite. *Proc. R. Soc. Lond. A* **459**, 2069–2076.

Harris P. J. F., Vis R. D. and Heymann D. (2000) Fullerene-like carbon nanostructures in the Allende meteorite. *Earth Planet. Sci. Lett.* **183**, 355–359.

Huss G. R. and Lewis R. S. (1994) Noble gases in presolar diamonds: I. Three distinct components and their implications for diamond origins. *Meteoritics* **29**, 791–810.

Huss G. R., Lewis R. S. and Hemkin S. (1996) The "normal planetary" noble gas component in primitive chondrites: compositions, carrier, and metamorphic history. *Geochim. Cosmochim. Acta* **60**, 3311–3340.

Lewis R. S., Srinivasan B. and Anders E. (1975) Host phase of a strange xenon component in Allende. *Science* **190**, 1251–1262.

Lewis R. S., Anders E. and Draine B. T. (1989) Properties, detectability and origin of interstellar diamonds in meteorites. *Nature* **339**, 117–121.

Marrocchi Y., Derenne S., Marty B. and Robert F. (2005) Interlayer trapping of noble gases in insoluble organic matter of primitive meteorites. *Earth Planet. Sci. Lett.* **236**, 569–578.

Matsuda J. and Amari S. (2009) Reexamination of the effect of pyridine treatment on phase Q in Orgueil. *Meteorit. Planet. Sci.* **44**, A134.

Matsuda J. and Yoshida T. (2001) The plasma model for the origin of the phase Q: an experimental approach and the comparison with the labyrinth model. *Meteorit. Planet. Sci.* **36**, A127.

Matsuda J., Kusumi A., Yajima H. and Syono Y. (1995) Noble gas studies in diamonds synthesized by shock loading in the laboratory and their implications on the origin of diamond in ureilites. *Geochim. Cosmochim. Acta* **59**, 4939–4949.

Matsuda J., Amari S. and Nagao K. (1999) Purely physical separation of a small fraction of the Allende meteorite that is highly enriched in noble gases. *Meteorit. Planet. Sci.* **34**, 129–136.

Matsuda J., Namba M., Maruoka T., Matsumoto T. and Kurat G. (2005) Primordial noble gases in a graphite-metal inclusion from the Canyon Diablo IAB meteorite and their implications. *Meteorit. Planet. Sci.* **40**, 431–443.

Matsuda J., Morishita K., Nara M. and Amari S. (2009) Raman spectroscopic study of the noble gas carrier Q in the Allende meteorite. *Geochem. J.* **43**, 323–329.

Matsuda J., Tsukamoto H., Miyakawa C. and Amari S. (2010) Noble gas study of the Saratov L4 chondrite. *Meteorit. Planet. Sci.* **45**, 361–372.

Matsuda J., Amari S., Morishita K., Nagashima K. and Nara M. (in press) The effect of pyridine treatment on phase Q: Orgueil and Allende. *Meteorit. Planet. Sci.*

Moniot R. K. (1980) Noble-gas-rich separates from ordinary chondrites. *Geochim. Cosmochim. Acta* **44**, 253–271.

Murty S. V. S. and Marti K. (1987) Nucleogenic noble gas component in Cape York iron meteorite. *Geochim. Cosmochim. Acta* **51**, 163–172.

Nakamura K., Zolensky M. E., Tomita S., Nakashima S. and Tomeoka K. (2002) Hollow organic globules in the Tagish Lake meteorite as possible products of primitive organic reactions. *Int. J. Astrobiol.* **1**, 179–189.

Nishimura C., Matsuda J. and Kurat G. (2008) Noble gas content and isotope abundances in phases of the Saint-Aubin (UNGR) iron meteorite. *Meteorit. Planet. Sci.* **43**, 1333–1350.

Orwa J. O., Nugent K. W., Jamieson D. N. and Prawer S. (2000) Raman investigation of damage caused by deep ion implantation in diamond. *Phys. Rev. B* **62**, 5461–5473.

Ott U. (2002) Noble gases in meteorites – trapped components. *Rev. Mineral. Geochem.* **47**, 71–100.

Ott U., Mack R. and Chang S. (1981) Noble-gas-rich separates from the Allende meteorite. *Geochim. Cosmochim. Acta* **45**, 1751–1788.

Ozima M. and Podosek F. A. (2002) *Noble Gas Geochemistry*. Cambridge University Press, Cambridge, UK, 286p.

Prawer S., Nugent K. W., Jamieson D. N., Orwa J. O., Bursill L. A. and Peng J. L. (2000) The Raman spectrum of nanocrystalline diamond. *Chem. Phys. Lett.* **332**, 93–97.

Remusat L., Le Guillou C., Rouzaud J.-N., Binet L., Derenne S. and Robert F. (2008) Molecular study of insoluble matter in Kainsaz CO3 carbonaceous chondrite: comparison with CI and CM IOM. *Meteorit. Planet. Sci.* **43**, 1099–1111.

Reynolds J. H., Frick U., Neil J. M. and Phinney D. L. (1978) Rare-gas-rich separates from carbonaceous chondrites. *Geochim. Cosmochim. Acta* **42**, 1775–1797.

Schelhaas N., Ott U. and Begemann F. (1990) Trapped noble gases in unequilibrated ordinary chondrites. *Geochim. Cosmochim. Acta* **54**, 2869–2882.

Smith P. P. K. and Buseck P. (1981) Graphitic carbon in the Allende meteorite: a microstructural study. *Science* **212**, 322–324.

Solin S. A. and Ramdas A. K. (1970) Raman spectrum of diamond. *Phys. Rev. B* **1**, 1687–1698.

Srinivasan B., Lewis R. S. and Anders E. (1978) Noble gases in the Allende and Abee meteorites and a gas-rich mineral fraction: investigation by stepwise heating. *Geochim. Cosmochim. Acta* **42**, 183–198.

Sun K. W., Wang J. Y. and Ko T. Y. (2008) Photoluminescence and Raman spectroscopy of single diamond nanoparticle. *J. Nanopart. Res.* **10**, 115–120.

Tuinstra F. and Koenig J. L. (1970) Raman spectrum of graphite. *J. Chem. Phys.* **53**, 1126–1130.

Ugarte D. (1992) Curling and closure of graphitic networks under electron-beam irradiation. *Nature* **359**, 707–709.

Verchovsky A. B., Sephton M. A., Wright I. P. and Pillinger C. T. (2002) Separation of planetary noble gas carrier from bulk carbon in enstatite chondrites during stepped combustion. *Earth Planet. Sci. Lett.* **199**, 243–255.

Vis R. D., Mrowiec A., Kooyman P. J., Matsubara K. and Heymann D. (2002) Microscopic search for the carrier phase Q of the trapped planetary noble gases in Allende, Leoville and Vigarano. *Meteorit. Planet. Sci.* **37**, 1391–1399.

Wacker J. F. (1989) Laboratory simulation of meteoritic noble gases: III. Sorption of neon, argon, krypton, and xenon on carbon: elemental fractionation. *Geochim. Cosmochim. Acta* **53**, 1421–1433.

Wacker J. F., Zadnik M. G. and Anders E. (1985) Laboratory simulation of meteoritic noble gases: I. Sorption of xenon on carbon: trapping experiments. *Geochim. Cosmochim. Acta* **49**, 1035–1048.

Wieler R., Anders E., Baur H., Lewis R. S. and Signer P. (1991) Noble gases in "phase Q": closed-system etching of an Allende residue. *Geochim. Cosmochim. Acta* **55**, 1709–1722.

Wieler R., Anders E., Baur H., Lewis R. S. and Signer P. (1992) Characterisation of Q-gases and other noble gas components in the Murchison meteorite. *Geochim. Cosmochim. Acta* **56**, 2907–2921.

Zadnik M. G., Wacker J. F. and Lewis R. S. (1985) Laboratory simulation of meteoritic noble gases: II. Sorption of xenon on carbon: etching and heating experiments. *Geochim. Cosmochim. Acta* **49**, 1049–1059.

Associate editor: Christian Koeberl